Scientific Data

https://doi.org/10.1038/s41597-025-06519-y

Article in Press

A Global High-Resolution Comprehensive Heat Indices Dataset from 1950 to 2024

Received: 7 August 2025

Accepted: 22 December 2025

Cite this article as: Malik, A., Masabathini, S., Shaikh, M.A. *et al.* A Global High-Resolution Comprehensive Heat Indices Dataset from 1950 to 2024. *Sci Data* (2025). https://doi.org/10.1038/s41597-025-06519-y

Abdul Malik, Sateesh Masabathini, Mohsin Ahmed Shaikh, Qinqin Kong, Muhammad Usman, Dasari Hari Prasad & Ibrahim Hoteit

A Global High-Resolution Comprehensive Heat Indices Dataset from 1950 to 2024

Abdul Malik[1], Sateesh Masabathini[1], Mohsin Ahmed Shaikh[2], Qinqin Kong[3], Muhammad Usman[4], Hari Prasad Dasari[1] & Ibrahim Hoteit[1]

[1]Climate Change Center, King Abdullah University of Science and Technology, Jeddah, Saudi Arabia.

[2]Supercomputing Lab, King Abdullah University of Science and Technology, Jeddah, Saudi Arabia.

[3]School of Medicine, Stanford University, Stanford, CA, US.

[4]College of Natural and Health Sciences, Zayed University, Abu Dhabi, United Arab Emirates

Heatwaves are becoming more intense and frequent as global temperatures rise, affecting vulnerable populations, particularly in low-income communities. Addressing the impacts of heatwaves requires high-resolution data to assess their influence on labour productivity, public health, and climate risk. We introduce the Comprehensive Heat Indices (CHI) dataset, a high-resolution (0.1° × 0.1°) hourly dataset from 1950 to 2024, derived from the ERA5 and ERA5-Land reanalyses. The CHI dataset encompasses thirteen heat stress indices, including wet-bulb temperature, universal thermal climate index, mean radiant temperature, wind chill, and lethal heat stress index (Ls). Thresholds for Ls are empirically linked to mortality, enabling the identification of life-threatening heat events. Ls is sensitive to soil moisture variability, improving assessments in agricultural regions. The CHI dataset supports indoor and outdoor applications and is sensitive to humidity, radiation, and wind. Covering the global land area from 60°S to 75°N and 180°W to 180°E, it provides a unique, long-term perspective on spatial and temporal trends in heat stress, which are critical for climate impact research and adaptation planning.

Background & Summary

Heat stress is the net heat burden an individual experiences, resulting from the combined thermal influences of environmental factors, including air and radiant temperatures, humidity, wind, and physical activity and clothing.[1,2] Understanding and mitigating heat stress impacts is crucial in rising global temperatures, especially given its implications for heat-related mortality[3,4,5,6,7,8,9,10] and reduced work capacity[11,12].

A good and useful heat stress dataset should provide fine spatial and temporal resolution with global coverage. Such a resolution is essential for accurately assessing heat stress and its spatial variability, capturing acute peak periods shaped by geography[13], vegetation[14,15], and meteorological factors[13]. The existing heat-stress datasets often fail to capture moisture-related dynamics and long-term trends across diverse climates, highlighting the need for more detailed, humidity-inclusive data and globally consistent frameworks[16]. A comprehensive heat stress dataset should also include a range of indices, as many currently in use vary in their structure. Some heat stress indices account for radiation and wind, while others do not. Some are tailored for dry environments, others for humid ones, and some follow linear relationships, while others follow nonlinear ones. As a result, different indices disagree on important questions, such as the effectiveness of evaporative cooling strategies (e.g., whether irrigation reduces or amplifies heat stress) due to their differing sensitivities to soil moisture. Although an ideal index would perform optimally across all conditions, no single index consistently outperforms the rest. Thus, selecting an appropriate heat index is crucial for assessing the impact of heat on human health[2]. Most heat stress indices are developed for specific environmental conditions[17] and should be used with caution in other contexts[18]. The choice of an optimal heat index depends on the usage context, as its suitability can vary across age groups, seasons, demographics, and geographic regions[19], and should therefore be selected accordingly.

Each heat index has its strengths and limitations, making it essential to incorporate multiple indices in a dataset to capture the uncertainty in heat-related impacts across diverse environmental conditions[2]. For instance, indices like Wet-Bulb Globe Temperature (Twbg) may not always adequately reflect human physiological responses to heat, potentially underestimating health risks. Twbg underestimates heat stress in low wind and high humidity conditions[18] and cannot capture the harmful effect of high wind in extremely hot and dry environments[20]. The Universal Thermal Climate Index (UTCI) provides a more robust assessment by focusing on human heat balance and offers a nuanced understanding of physiological responses to thermal conditions[2]. However, UTCI struggles to provide accurate results under certain climatic conditions, particularly in environments with significant microclimatic variations, such as urban areas, where it may yield inconsistent assessments, thereby complicating public health and occupational safety decision-making processes[21]. Further, the UTCI is undefined under extreme conditions, specifically when the water vapour pressure is less than or equal to 5 kPa, the air temperature exceeds ±50 °C, or the difference between the mean radiant temperature (Tmrt) and the 2-metre air temperature (T2m) lies between –30 °C and 70 °C.[22] Moreover, for most conditions, UTCI responds less to humidity changes than Wet-Bulb Temperature (Twb), with Twb being more humidity-sensitive, especially at lower temperatures and lower humidity[23]. Thus, providing a wide range of heat stress metrics is crucial to allow users to select the one that best suits their application scenarios.

Current heat stress datasets, while valuable, have notable limitations. For instance, the ERA5-HEAT[22] (Human thErmAl comforT) dataset provides Tmrt and UTCI derived from the ERA5 reanalysis[24] since 1940, at a spatial resolution of 31 km and an hourly temporal resolution. Although ERA5-HEAT[22] offers global coverage, it lacks a comprehensive suite of heat-stress indices essential for assessing heat-related impacts at high resolution across different climates. Studies like those by Yan et al.[1] and Spangler et al.[25] have focused on specific regions with daily indices at a fine spatial resolution of 0.1° × 0.1°; however, they do not offer comprehensive global coverage or the hourly resolution necessary for detailed night-time heat stress assessments, which are crucial for understanding diurnal temperature effects on human health[26]. Jian et al.[27] recently utilised ERA5-Land[28,29] and ERA5[24] to compute the UTCI. However, while global from 2000 to 2023, their dataset lacks a diverse set of indices and comprehensive historical coverage from 1950.

The mortality-based human lethal heat stress index[30] (Lsi) is an empirical index that links air temperature, humidity, and heatwave-related deaths. Derived from Twb, a physical measure of the body's cooling limit under given atmospheric conditions[30], Lsi outperforms indices like UTCI, Heat Index (HI), Humidex (Hu), and Twbg in identifying dangerous heatwave days, particularly in low-humidity conditions[31]. Since Twb tends to rise in irrigated areas[32], soil moisture plays a key role in lethal heat stress. It can increase risk in irrigated regions[30] since wet soils lower temperature but raise humidity, while dry soils raise temperature and reduce humidity, both of which can worsen heat stress[30,33]. The increased sensitivity of Lsi to humidity offers a more accurate reflection of heat stress in diverse climates, especially in agricultural zones. Therefore, we calculated and provided global Lsi estimates in this study.

Thus, to overcome the abovementioned gaps, the present work introduces the Comprehensive Heat Indices (CHI) dataset, which aims at enhancing the accuracy of existing heat stress datasets by using 2-m wind speed instead of the commonly used 10-meter wind speed and by calculating the average cosine of the solar zenith angle (cosθ) only over the sunlit part of each model interval. In contrast, previous studies use 10-meter wind speed[1,25] and average cosθ[1,22,25,27] over the employed model interval. The 2-m wind speed better captures near-surface conditions relevant to human heat stress than the 10-m wind speed, which is measured higher above ground. For instance, an increase in wind speed from 0.5 m/s to 1.5 m/s can lead to a median Twbg decrease of 2.3°C[34], indicating that even modest changes in wind speed can significantly impact Twbg calculations. Using sunlit-only cosθ prevents overestimation of solar radiation and unrealistic spikes in heat-stress indices. In Yan et al.[1], the Twbg was calculated under indoor conditions and does not account for the effects of solar radiation, rendering it incompatible with outdoor heat stress assessments. In the CHI dataset, we explicitly calculate outdoor Twbg, incorporating full radiation inputs. Additionally, while Yan et al.[1] estimated indoor Twb using the Stull[35] approximation, we provide both indoor and natural wet-bulb temperatures (Tnwb) using the physically-based model of Liljegren et al.[36]. Moreover, Yan et al.[1] do not offer heat stress indices such as globe temperature (Tg), Tnwb, Lsi, and outdoor Twbg for their Southeast Asia study region. Similarly, Spangler et al.[25] do not provide key thermal indices, including Tg, Tnwb, Tmrt, Twb, apparent temperature (AT), wind chill (WC), and HI.

Moreover, the impacts of global warming are profoundly felt and projected in poor and low-income countries[37], particularly in the tropics and subtropics[12,38]. Regions such as the Middle East and North Africa are experiencing rapid warming[39], facing heat-related mortalities[5], and lack high-resolution data. This gap highlights the urgent need for data to monitor and analyse the precise impacts of heat stress in these vulnerable regions.

Therefore, we introduce CHI as the first long-term (1950-2024) comprehensive and diverse dataset of high-resolution heat stress indices derived from ERA5 and ERA5-Land reanalyses, offering hourly resolution with a 9 km grid (0.1° × 0.1°). We provide a set of 13 heat stress indices (Tmrt, Tg, Twbg, UTCI, Twb, Tnwb, indoor and outdoor Lsi, Hu, NET, AT, WC, HI) suitable for diverse environmental conditions to assess heat-related impacts. Importantly, our study provides the first dataset on Lsi, addressing critical gaps in regional heat stress research. This dataset aims to enhance the accuracy of heat stress assessments by providing crucial insights into the temporal and spatial dynamics of heat stress and its impacts, particularly in under-resourced regions vulnerable to climate extremes.

Methods

Input Data Description

We utilised two high-resolution global reanalysis products developed by the European Centre for Medium-Range Weather Forecasts (ECMWF) to calculate heat stress indices. These are: (i) ERA5[24,40] (https://cds.climate.copernicus.eu/datasets/reanalysis-era5-single-levels?tab=overview), the fifth generation of European reAnalysis, and (ii) ERA5-Land[28,29,41] (https://cds.climate.copernicus.eu/datasets/reanalysis-era5-land?tab=overview). Both reanalyses from the Copernicus Climate Change Service (C3S) provide data at an hourly temporal resolution. ERA5 combines model output with various observational datasets through data assimilation, providing a spatial resolution of 31 km (0.25° × 0.25°)[24,40]. ERA5-Land, on the other hand, provides a finer spatial resolution of 9 km (0.1° × 0.1°). It is generated by integrating the ECMWF land surface model at high resolution globally, using downscaled meteorological inputs (air temperature, pressure and humidity) from the ERA5 climate reanalysis. It includes an elevation correction to accurately represent the thermodynamic state near the surface[29]. We used both reanalysis products from 1950 to 2024 at an hourly resolution.

As detailed in Table 1, various atmospheric variables were required to calculate heat stress indices. All variables in Table 1 were obtained from ERA5-Land, except for the total sky direct solar radiation (tsdsrs), which was sourced from ERA5, as ERA5-Land does not provide this variable. The tsdsrs was interpolated onto the ERA5-Land grid to ensure consistency across all variable grids following Yan et al.[1] and Spangler et al.[25]. The nearest-neighbour method was employed because it conserves the original data values[1]. Some other variables listed in Table 2, such as relative humidity (rh), cosθ, wind speed at 2 m (ws2), direct radiation from the sun (dsrp), and the ratio of direct solar radiation (fdir), were calculated from the variables listed in Table 1.

Data for Technical Validation

To evaluate the quality of the CHI dataset, we compare it with three existing gridded heat stress index datasets: ERA5-HEAT[22,42] (https://cds.climate.copernicus.eu/datasets/derived-utci-historical?tab=overview) at 0.25° × 0.25° resolution, HiTiSEA[1,43] (High-spatial-resolution Thermal-stress Indices over South and East Asia; https://doi.org/10.6084/m9.figshare.c.5196296) at 0.1° × 0.1°, and HiGTS[27,44] (High temporal resolution Global Thermal Stress metrics; https://figshare.com/collections/HiGTS_A_high-resolution_global_gridded_dataset_of_human_thermal_stress_indices/6948135), also at 0.1° ×

0.1° resolution. To see the differences between the CHI dataset and ERA5-HEAT, the ERA5-HEAT data were bilinearly interpolated to a 0.1° × 0.1° spatial resolution.

We use daily maximum values of UTCI and Tmrt from ERA5-HEAT and UTCI from HiGTS for comparison with CHI data over the geographic domain 60°S–75°N and 180°W–180°E. Additionally, we compare Tmrt, WC, UTCI, Twb, Hu, NET, AT, and HI from HiTiSEA with corresponding CHI outputs over South and East Asia (SEA; 3°N–58°N, 65°E–155°E).

Codes Used for Calculating Heat Stress Indices

We calculated 13 heat stress indices, as detailed in Table 3, utilising established methods and already published codes with some modifications. Specifically, we integrated codes developed by Brimicombe et al.[45] and Kong et al.[46] to compute these indices.

Brimicombe et al.[45] developed thermofeel, a Python library from ECMWF, which facilitates the computation of various heat stress indices. thermofeel employs the same methods as those used for ERA5-Heat[22] to calculate Tmrt and UTCI. thermofeel is available for download on GitHub (https://github.com/ecmwf/thermofeel), and comprehensive documentation, including a user guide, can be found in the thermofeel documentation (https://thermofeel.readthedocs.io/en/latest/).

On the other hand, Kong et al.[46] developed a Python code (https://zenodo.org/records/5980536) to calculate various heat stress indices, with a primary focus on Tnwb and Twbg. This code enhances the earlier formulation by Liljegren et al.[36], which relied solely on surface solar radiation downward (ssrd) as the radiation input. Kong et al.[45] expanded this by incorporating five radiation components (see Table 1) into the method developed by Liljegren et al.[36]. This modification provides a more comprehensive and accurate calculation using a complete set of radiation inputs. For detailed information on these components and their application in calculating Tnwb and Twbg, refer to Tables 1–3.

Hourly Solar Radiation Conversion: J/m^2 to W/m^2

The five radiation components listed in Table 1 were available from C3S as hourly-accumulated energy, measured in joules per square meter (J/m^2). To calculate the heat stress metrics, we transformed this accumulated energy into average power flux, $P(t)$, in watts per square meter (W/m^2). The conversion was done as follows[47]:

$$P(t) = \frac{E(t) - E(t-1)}{\Delta t} \qquad (1)$$

$E(t)$ = Energy measured in J/m^2 at time t.

$E(t) - E(t-1)$ = Change in accumulated energy from the previous hour to the current hour

Δt = 3600 s (time interval in seconds over which the energy difference was calculated)

The solar radiation accumulated up to the first hour of the day was directly divided by Δt to get the average power flux for the first hour (https://confluence.ecmwf.int/pages/viewpage.action?pageId=197702790).

Cosine of the Solar Zenith Angle ($\cos\theta$)

For calculating Tmrt and Tnwb, cosθ was required as an input variable (Table 3) as it affects the amount of solar radiation a standing person receives[22]. The cosθ converts direct solar radiation from a flux passing through a horizontal plane to a plane perpendicular to the incoming solar rays[46,47]. This conversion can be done by dividing tsdsrs with cosθ (Table 2). Since ERA5 reanalyses radiation data are accumulated hourly, cosθ was required for each interval[46]. If the interval includes sunrise or sunset time, zeros from sun-below-horizon periods can make cosθ too small, leading to overestimated solar radiation and spiked values of heat stress indices that depend on radiation components[46,48]. Following Kong et al.[46] and using their code, we averaged cosθ only during the sunlit portion of the hourly interval. Kong et al.[46] employed the method described by Di Napoli et al.[47] to calculate cosθ (Table 2).

Calculation of Heat Stress Indices

We calculated all heat stress indices using thermofeel[45], except for Tnwb, which was calculated using the code provided by Kong et al.[46]. The following section outlines the methods and equations used to calculate heat stress indices.

Mean Radiant Temperature (Tmrt)

The Tmrt for a person in a specific environment, posture, and clothing is defined as the uniform temperature of an imaginary black-body enclosure (with an emissivity ε = 1) that would produce the same net radiant energy exchange with the person as the actual, more complex radiative surroundings[47,49]. Tmrt reflects how humans perceive thermal radiation (total net shortwave and longwave radiation) from their surroundings[22,50]. We calculated the Tmrt using the framework described by Di Napoli et al.[47], which was also used to produce ERA5-Heat[22],[42]. This framework computes Tmrt globally for a human body exposed to both direct and diffuse components of short-wave and longwave radiation, and it accounts for variations in the sun's position during the numerical model's accumulation interval. Incorporating the direct solar radiation from the sun (dsrp; see Table 2), the Tmrt was calculated using the following equation[47,51].

$$Tmrt = \left\{\frac{1}{\sigma}\left[f_a \times strd + f_a \times stru + \frac{a_{ir}}{\varepsilon_p}\left(f_a \times ssrdDif + f_a \times ssru + f_p \times dsrp\right)\right]\right\}^{0.25} \quad (2)$$

Where σ is the Stefan–Boltzmann constant (5.67×10^{-8} W/m^2K^4), strd is surface thermal radiation downwards, stru is surface thermal radiation upwards, ssru is surface solar radiation upwards (reflected), ssrdDif is the diffuse component of the surface solar radiation downwards (ssrd). When exposed to solar radiation, the human body surface, including clothing and skin, is assumed to have a shortwave absorptance (α_{ir}) of 0.7 and a longwave emissivity (ε_p) of 0.97[51].

f_p is the surface projection factor, representing the fraction of the body surface directly exposed to solar radiation. This factor depends on the angle of incoming radiation (γ) relative to body posture. The posture considered is that of a standing or walking person, assumed to be rotationally symmetric[47,52,53]. In most cases, the detailed structure of a person's surrounding environment is unknown. Therefore, the person is assumed to be on an unshaded horizontal plane with equal solid angles (f_a) of 0.5 assigned to both the sky and the surrounding surface[51].

$f_p = 0.308\,cos\left(\gamma(0.998 - \gamma^2/50000)\right)$[54], $\gamma = 90^{\circ} - \theta$: solar elevation angle, and $\theta =$ solar zenith angle during only the sunlit part of the interval, which is the angle between the zenith and centre of the sun's disc and affects the amount of solar radiation received by a standing person[47].

Globe Temperature (Tg)

Tg is the equilibrium temperature measured at the centre of a black-painted, hollow copper sphere that absorbs radiant heat from all directions[55]. It was designed to reflect the temperature perceived by humans, capturing the combined effects of radiation, air temperature, and wind [55]. Tg is often used as input to calculate heat stress indices, especially the Twbg. However, a significant challenge in estimating the Twbg from meteorological data is the lack of Tg measurements at most weather stations worldwide[56,57]. Tg has some limitations. Increased air movement can raise Tg in cold environments, leading to an incorrect perception of improved comfort when the actual sensation is colder. Furthermore, when air and surrounding surfaces are at the same temperature, Tg remains unchanged with varying wind speeds, despite increased wind affecting thermal sensation[17]. thermofeel calculates Tg by solving the equation from Brimicombe et al.[48] using Tmrt, T2m, and ws2 as inputs.

$$Tmrt = \sqrt[4]{T_g^4 + \frac{h_{cg}}{\varepsilon \times D^{0.4}} \times \left(T_g - T2m\right)} \quad (3)$$

where, $h_{cg} = 1.1 \times 10^8 \times ws2^{0.6}$ (mean convective coefficient), ε is the emissivity of the globe, and D is the globe's diameter.

Universal Thermal Climate Index (UTCI)

UTCI is a biometeorological index that quantifies the physiological response of the human body to an outdoor thermal environment. It is defined as the temperature of a reference environment that would elicit the same dynamic physiological response as the actual environment[58]. UTCI expresses how hot or cold a person feels based on air temperature, wind speed, humidity, and radiant heat (Tmrt), using a detailed thermophysiological model of the human body. The UTCI was calculated using the same method as for ERA5-Heat by Di Napoli et al.[22]. In ERA5-Heat, UTCI was based on the approximation function developed by Bröde et al.[59] using the following sixth-order polynomial regression function[27,59]:

$$UTCI = T2m + f(T2m, \mathrm{ws10}, \mathrm{Tmrt}, \mathrm{e}) \tag{4}$$

Where f is the offset between UTCI and T2m ($i.e.,\ Tmrt - T2m$) calculated using sixth-order polynomial regression[27], and it depends on T2m, Tmrt, wind speed, and humidity, expressed as either water vapour pressure (e) or rh[59]. The physiological model used to calculate UTCI includes a formula that converts wind speed measured at 10 meters to wind speed at the body level[59]. Therefore, we use the 10-meter wind speed as input for UTCI calculation.

Natural Wet-bulb Temperature (Tnwb)

Tnwb is measured using a sensor fitted with a wetted wick that is fully exposed to the environment, allowing it to respond to heat transfer via evaporation, solar radiation, and convection[36,60]. Thus, Tnwb is a useful proxy for assessing how environmental conditions affect the body's ability to cool through sweating[36]. The Tnwb was calculated using the following equation:

$$Tnwb = T2m - \frac{\Delta H}{c_p}\frac{M_{H2O}}{M_{Air}}\left(\frac{Pr}{Sc}\right)^{0.56}\left(\frac{e_w - e_a}{P - e_w}\right) + \frac{\Delta F_{net}}{Ah} \tag{5}$$

where,

$$\Delta F_{net} = \frac{1}{2}\pi DL\varepsilon_w(strd + stru) - \pi DL\sigma\varepsilon_w T_w^4 + \left(\pi DL + \frac{\pi D^2}{4}\right)(1-\alpha_w)(1 - fdir)ssrd + \left(DL\sin\theta + \frac{\pi D^2}{4}\cos\theta\right)(1-\alpha_w)fdir\frac{ssrd}{\cos\theta} + \pi DL(1-\alpha_w)ssru \tag{6}$$

Where, ΔH: Latent heat of vaporisation of water; c_p: specific heat capacity of dry air; M_{H2O}: molar mass of water vapour; M_{air}: molar mass of dry air; Pr: Prandtl number; Sc: Schmidt number; e_w: vapour pressure at the wick surface (Pa); e_a: ambient vapour pressure; P: surface pressure (Pa); ΔF: net radiative gain by the wick; D: diameter of the wick or globe; L: length of the wick; ε_w: emissivity of the wick surface; α_w: albedo of the wick; fdir: ratio of the direct solar radiation; A: surface area of the wick; h: convective heat transfer coefficient. In the original physical model of

Liljegren et al.[36], the radiation components, such as strd, stru, ssru, and fdir, were approximated due to data limitations[46]. In contrast, the present study uses these components directly, as they are readily available, eliminating the need for approximation.

Indoor or Shaded Wet-bulb Temperature (Twb)

Twb is measured as a function of T2m and rh by following an empirical expression developed by Stull[35]:

$$Twb = T2m\ atan\left[0.151977(rh\% + 8.313659)^{\frac{1}{2}}\right] + atan(T2m + rh\%) - atan(rh\% - 1.676331) + 0.00391838(rh\%)^{\frac{3}{2}}\ atan(0.023101rh\%) - 4.686035 \quad (7)$$

where, $5\% \geq rh \leq 99\%$ and $-20℃ \leq T2m \leq 50℃$.

Lethal Heat Stress Index (Lsi)

The Lsi captures the relationship between temperature, humidity, and heatwave-related mortality while remaining comparable to the physical wet-bulb metric. It enables the assessment of how soil drying affects fatal heat stress across various climates[30]. Wouters et al.[30] defined Lsi by the following equation:

$$Lsi = Twb + 4.5\left(1 - \left[\frac{rh}{100}\right]^2\right) \quad (8)$$

[Figure 1 goes here]

The adjustment term 4.5(1−[rh/100]^2) was added to improve Twb under low humidity conditions. This term becomes zero at 100% relative humidity (rh), at which point cooling by sweating is no longer effective[30]. Wouters et al.[30] used Twb to calculate Lsi in equation (8); however, we present two versions: one using Twb for indoor or shaded conditions and another using Tnwb, which improves accuracy by accounting for wind and radiation effects for outdoor conditions. We refer to the latter as the natural lethal heat stress index (Lsin).

Wet-Bulb Globe Temperature (Twbg)

Twbg was developed for the US Army to assess heat stress risk under direct sunlight and to guide protective measures to prevent heat-related risks[36,61]. Twbg is widely used for monitoring the impacts of heat stress on public health[62], labour productivity[45], and sports activities[63]. Simple approximations of Twbg largely overestimate heat stress in hot and humid conditions and underestimate it in subtropical dry regions[46]. Therefore, we utilise the physically based Twbg model developed by Liljegren et al.[36] and modified by Kong et al.[46] to incorporate the influence of direct solar radiation. The outdoor Twbg was calculated as a weighted sum of Tnwb, Tg, and T2m, as shown in the following equation (9)

$$Twbg = 0.7 \times Tnwb + 0.2 \times Tg + 0.1 \times T2m \qquad (9)$$

Humidex (Hu)

Hu is an index developed in Canada to quantify how hot it feels to a person, considering both air temperature and humidity[64]. The Hu is defined as a number that represents the perceived temperature, taking into account both the actual air temperature and the moisture content in the air[64]. It was calculated using the following equation (10)[64]:

$$Hu = T2m + \frac{5}{9}(e - 10) \qquad (10)$$

Where e is the vapour pressure of water. Hu can be easily calculated from two meteorological parameters, T2m and Td2m, and its value is always equal to or greater than T2m[64].

Normal Effective Temperature (NET)

NET is a thermal comfort index that combines T2m, rh, and ws2 into a single value, reflecting human thermal stress in both hot and cold conditions[65]. It is expressed by the following equation (11)[65]:

$$NET = 37 - \frac{37 - T2m}{0.68 - 0.0014\ \times rh + \frac{1}{(1.76 + 1.4 \times ws1.2^{0.75})}} - 0.29 \times T2m(1 - 0.01 \times rh) \qquad (11)$$

Thermofeel calculates the wind speed at 1.2 m (ws1.2) by equation (12).

[Figure 2 goes here]

$$ws1.2 = ws10\left(\frac{log_{10}\left({}^{1.2}/_{z_0}\right)}{log_{10}\left({}^{10}/_{z_0}\right)}\right) \qquad 12$$

Z_0 is the surface roughness length, set to 0.01 m, representing smooth open terrain. Like wind chill and apparent temperature, NET rises with higher temperature and humidity in hot weather but drops with stronger winds. In cold weather, NET decreases as temperature drops and humidity and wind speed increase[65].

Apparent Temperature (AT)

AT is calculated using the empirical equation (4), which approximates the perceived temperature to the human body based on T2m, rh, and wind speed. The AT adjusts the T2m based on air moisture content, which affects the evaporative cooling capacity of the human body[66].

$$AT = T2m + 0.33 \times rh - 0.70 \times ws1.2 - 4 \quad (13)$$

The thermofeel takes ws10 as input and converts it to wind speed at 1.2 m (ws1.2) using the following empirical approximation.

$$ws1.2 = ws10 \times \frac{4.87}{\ln(67.88 \times zws - 5.42)} \quad (14)$$

Where zws is the height at which the wind speed was measured (here, 10 m), thus, AT provides heat stress values at human height.

Wind Chill (WC)

WC quantifies heat loss from the human body caused by the combined effects of wind and low temperatures in cold environments[67]. It estimates the cooling power of the atmosphere, reflecting how cold it feels to the human body when exposed skin is subjected to cold air and wind[68]. WC was calculated using the equation (15) given in Coccolo et al.[68]:

$$WC = 13.12 + 0.6215 \times T2m - 11.37 \times ws2^{0.16} + 0.3965 \times T2m \times ws2^{0.16} \quad (15)$$

While useful in cold, windy conditions, WC overlooks solar radiation and individual characteristics, overestimating cooling for bare skin and underestimating it for clothed individuals[68].

Heat Index Adjusted (HI)

Heat Index Adjusted is a measure of human-perceived equivalent temperature that accounts for air temperature and humidity, with correction terms applied under specific extreme conditions to enhance accuracy, as described by the US National Weather Service (NWS) methodology. The HI equation[69] (Eq. 16) was developed using multiple regression analysis of T2m and rh, based on the original version of Steadman[66,70]. thermofeel calculates HI using the Rothfusz[69]

[Figure 3 goes here]

[Figure 4 goes here]

regression equation and applies three adjustments to it under specific conditions described by the US NWS (https://www.wpc.ncep.noaa.gov/html/heatindex_equation.shtml). The Rothfusz[69] empirical regression equation for HI is as follows:

$$\begin{aligned} HI_R = {} & -42.379 + 2.04901523 \times T2m + 10.1433312 \times rh - 0.22475541 \times T2m \times rh \\ & - 0.00683783 \times T2m^2 - 0.05481717 \times rh^2 + 0.00122874 \times T2m^2 \times rh \\ & + 0.00085282 \times T2m \times rh^2 - 0.00000199 \times T2m^2 \times rh^2 \end{aligned} \quad (16)$$

Adjustment 1 is an initial approximation for low heat index values when environmental conditions are not excessively hot or humid, and a simplified formula is used to estimate the heat index more appropriately.

$$HI_{initial} = 0.5 \times (T2m + 61 + 1.2(T2m - 68) + 0.94 \times rh) \tag{17}$$

$$T_{avg} = \frac{T2m + HI_{initial}}{2} \tag{18}$$

If T_{avg} < 80°F, then $HI = HI_{initial}$; otherwise, $HI = HI_R - Adjustment[2\ or\ 3]$, i.e. subtract Adjustment 2 or 3 from HI_R based on T2m and rh values.

Adjustment 2 (Low humidity, high temperature) applies if rh < 13% and 80°F < T2m < 112°F

$$HI = HI_R - \left(\frac{13 - rh}{4}\right) \times \sqrt{\frac{17 - |T2m - 95|}{17}} \tag{19}$$

Adjustment 3 (high humidity, moderate temperature) applies if rh < 85% and 80°F < T2m < 87°F

$$HI = HI_R - \left(\frac{rh - 85}{10}\right) \times \left(\frac{87 - T2m}{5}\right) \tag{20}$$

Data Records

The CHI[71] dataset is provided in NetCDF format, with monthly files containing hourly data for each heat index. Each monthly file is approximately 5.6 GB, totalling roughly 73 TB and 11,700 files over 75 years (1950-2024). The CHI[71] data are available for access and download via Globus (https://www.globus.org/), hosted in the KAUST (King Abdullah University of

[Figure 5 goes here]

Science & Technology) Data Repository – Datawaha. To download the data, users must sign in to Globus using one of the following options: a Globus ID, ORCID, GitHub, Google account, or institutional credentials. The user can freely access the data, along with the user guide, description, and metadata from https://doi.org/10.6084/m9.figshare.30539867.

Each heat index dataset spans from 00:00 UTC on January 2, 1950, to 23:00 UTC on December 31, 2024. Files follow the naming convention: CHI_<IndexName>_YYYY-MM.nc, where

<IndexName> is the abbreviation of the specific index as listed in Table 3. For example, the file containing UTCI data for June 2015 would be named: CHI_UTCI_2015-06.nc.

Technical Validation

A comprehensive technical validation of the generated heat stress indices would require high-quality, globally observed gridded or station-based data, which is not thoroughly available for all indices. However, the ECMWF reanalysis products (ERA5[24] and ERA5-Land[28,29]), the computational methods, and the codes[45,46] used in this study are well documented, widely accepted, and have been previously validated[25]. Therefore, in this work, we present maps of each heat stress index for January and July, shown as daily maximum values, except for WC, which is presented as both daily minimum and maximum. All results are averaged over the 1950–2024 period, and we include their averaged spatial range from minimum to maximum. We encourage users to conduct region-specific validation using locally available observational data, depending on their geographic location and application context.

Figures 1 and 2 present the daily maximum values for January and July, respectively, averaged from 1950 to 2024, for all calculated heat stress indices except the WC index. These figures also illustrate the average global spatial range of each index. Figure 3 displays the daily minimum and maximum WC values for the same months and period. These figures demonstrate that all heat stress indices have been reliably computed, with their spatially averaged minimum and maximum values falling within physically reasonable and valid ranges. As expected, Lsin exhibits higher values than Lsi due to the inclusion of radiative effects, which Lsi does not account for.

We compare the CHI[71] dataset with ERA5-Heat[22] and HiGTS[27] for the global heatwave on June 20, 2015 (Figs. 4–5). This date was selected due to a widespread heatwave event affecting parts of Europe, North America, Asia, and South America[72]. CHI's UTCI is compared with ERA5-Heat and HiGTS (Figs. 4a, c, e and 5a, c, d, f), while Tmrt is compared only with ERA5-Heat (Figs. 4b, d and 5b, e).

Figure 4 shows that CHI successfully captures the spatial pattern of the heatwave and aligns well with ERA5-Heat and HiGTS. However, Figure 5 reveals notable differences in colder regions such as Greenland, Canada, the Tibetan Plateau, northern Russia, and southern South America. The differences between CHI and ERA5-Heat (HiGTS) for UTCI range between -22.3 (-6.5) and +20 (+10) °C, respectively. These discrepancies may arise from differences in

[Figure 6 goes here]

spatial resolution—CHI at 0.1° versus ERA5-Heat at 0.25°—which can smooth terrain, alter coastal gradients, and affect wind fetch, contributing to spatial differences. Interpolation to a common grid can also introduce artificial warm/cool biases around steep terrain or coastlines, appearing as positive or negative UTCI differences.

We present histograms of the bias distribution (Fig. 5d–f), which show that the 95th and 99th percentile differences of CHI UTCI relative to ERA5-Heat (HiGTS) UTCI are 2.49°C (1.21°C) and 4.57°C (2.49°C), respectively, indicating that only a small fraction of grid points exhibit larger differences. For Tmrt, the corresponding 95th- and 99th-percentile biases are 2.9°C and 6.8°C, respectively.

Figure 6 compares CHI with HiTSEA for the heat stress indices common to both datasets on June 10, 2019, during a severe heatwave over India and Pakistan. Both datasets show consistent spatial patterns, capturing the extent and intensity of the heatwave across all indices. Most indices exhibit near-zero bias across the region; however, larger differences are noticeable for Tmrt and UTCI, particularly over the Tibetan Plateau and other relatively colder areas (Fig. 7). These differences may be attributed to CHI using 2 m wind speed. In contrast, HiTSEA uses 10 m wind speed (except for UTCI and NET), which can influence convective cooling. Also, HiTSEA applies a slightly different formulation for the projected area factor, f_p, which may contribute to these differences in Tmrt and UTCI.

These differences are particularly pronounced because the comparison focuses on a single heatwave event. Such discrepancies would likely decrease over extended periods, such as for annual or multi-year averages.

Usage Notes

We provide high-resolution hourly data for 13 heat stress indices from 1950 to 2024, suitable for assessing both heat and cold waves for indoor and outdoor environments across diverse climatic conditions and applications. Each index has its own range of normal-to-extreme threshold values to evaluate heat stress. Further details on interpretation scales can be found in the thermofeel[45] documentation (https://thermofeel.readthedocs.io/en/latest/) and related studies[70,73].

Wouters et al.[30] identified two key thresholds for Lsi, derived from global mortality data: Lsi = 19°C indicates the onset of excess mortality ("lethal"), while Lsi = 27°C reflects conditions where mortality becomes highly likely ("deadly"). These thresholds are based on daily mean values and align well with historical patterns of heatwave mortality.

Indices such as Twb, Lsi, Hu, NET, AT, and HI are most applicable to indoor or shaded environments, while UTCI, Tnwb, Lsin, and Twbg are better suited for assessing outdoor, radiation- and wind-exposed conditions. The Lsi and Lsin indices are particularly relevant for evaluating heat-related risks in low-humidity areas, including agricultural zones, arid regions, and wetlands.

[Figure 7 goes here]

The CHI dataset supports multidisciplinary applications in climate science, public health, labour productivity, climate risk assessment and adaptation planning, as well as indoor and outdoor heat-stress assessment.

The urban heat island (UHI) effect, which refers to the temperature difference between urban areas and their surrounding rural areas[74], intensifies heat stress, posing a significant threat to

vulnerable populations[75]. While high-resolution data is ideal for identifying intra-urban heat hotspots, moderate-resolution datasets, such as 9 km, are effective for regional-scale heat island characterisation. Although Tmrt has a spatial resolution of 9 km, it still offers advantages over air or surface temperatures by accounting for radiative effects more comprehensively[50,76]. Thus, CHI Tmrt data and complementary heat indices can enable comparative assessments of broad regional thermal contrasts.

Data Availability

The user can freely access the data, along with the user guide, description, and metadata from https://doi.org/10.6084/m9.figshare.30539867.

Code Availability

The Python library thermofeel[45], used to calculate most of the heat stress indices, is freely available on GitHub at https://github.com/ecmwf/thermofeel. We used thermofeel to compute rh and all heat indices except Tnwb. For Tnwb, along with variables such as cos θ, ws10, ws2, dsrp, and fdir, we utilised the Python code developed by Kong et al.[46], which is available at https://zenodo.org/records/5980536. Both the thermofeel[45] and Kong et al.[46] codes were optimised and adapted to meet the requirements of CHI dataset production. The modified and integrated version of these codes is available for download and further use from the GitHub repository at https://github.com/masabhathini/CHIdatasets.

References

1. Yan, Y., Xu, Y. & Yue, S. A high-spatial-resolution dataset of human thermal stress indices over South and East Asia. *Sci. Data* **8**, 1–14 (2021).
2. Vanos, J. K., Baldwin, J. W., Jay, O. & Ebi, K. L. Simplicity lacks robustness when projecting heat-health outcomes in a changing climate. *Nat. Commun.* **11**, 10–14 (2020).
3. Chen, H. *et al.* Projections of heatwave-attributable mortality under climate change and future population scenarios in China. *Lancet Reg. Heal. - West. Pacific* **28**, 1–11 (2022).
4. Gasparrini, A. *et al.* Projections of temperature-related excess mortality under climate change scenarios. *Lancet Planet. Heal.* **1**, e360–e367 (2017).
5. Hajat, S., Proestos, Y., Araya-Lopez, J. L., Economou, T. & Lelieveld, J. Current and future trends in heat-related mortality in the MENA region: a health impact assessment with bias-adjusted statistically downscaled CMIP6 (SSP-based) data and Bayesian inference. *Lancet Planet. Heal.* **7**, e282–e290 (2023).

6. Mathers, C. D. & Loncar, D. Projections of global mortality and burden of disease from 2002 to 2030. *PLoS Med.* **3**, 2011–2030 (2006).
7. Vicedo-Cabrera, A. M. *et al.* Temperature-related mortality impacts under and beyond Paris Agreement climate change scenarios. *Clim. Change* **150**, 391–402 (2018).
8. Wu, Y. *et al.* Global, regional, and national burden of mortality associated with short-term temperature variability from 2000–19: a three-stage modelling study. *Lancet Planet. Heal.* **6**, e410–e421 (2022).
9. Yang, J. *et al.* Projecting heat-related excess mortality under climate change scenarios in China. *Nat. Commun.* **12**, 1–11 (2021).
10. Zhao, Q. *et al.* Global, regional, and national burden of mortality associated with non-optimal ambient temperatures from 2000 to 2019: a three-stage modelling study. *Lancet Planet. Heal.* **5**, e415–e425 (2021).
11. Andrews, O., Le Quéré, C., Kjellstrom, T., Lemke, B. & Haines, A. Implications for workability and survivability in populations exposed to extreme heat under climate change: a modelling study. *Lancet Planet. Heal.* **2**, e540–e547 (2018).
12. Masuda, Y. J. *et al.* Impacts of warming on outdoor worker well-being in the tropics and adaptation options. *One Earth* **7**, 382–400 (2024).
13. Li, W., Chao, L., Si, P., Zhang, H. & Li, Q. Comparisons of the Urbanization Effect on Heat Stress Changes in Guangdong during Different Periods. *Remote Sens.* **15**, (2023).
14. Rahman, M. A. *et al.* Spatial and temporal changes of outdoor thermal stress: influence of urban land cover types. *Sci. Rep.* **12**, 1–13 (2022).
15. Wang, C. *et al.* Satellite-based mapping of the Universal Thermal Climate Index over the Yangtze River Delta urban agglomeration. *J. Clean. Prod.* **277**, 123830 (2020).
16. Mohammad, P. & Weng, Q. Comparing existing heat wave indices in identifying dangerous heat wave outdoor conditions. *Nexus* **1**, 100027 (2024).
17. Macpherson, R. K. The assessment of the thermal environment. A review. *Br. J. Ind. Med.* **19**, 151–164 (1962).
18. Budd, G. M. Wet-bulb globe temperature (WBGT)-its history and its limitations. *J. Sci. Med. Sport* **11**, 20–32 (2008).
19. Barnett, A. G., Tong, S. & Clements, A. C. A. What measure of temperature is the best predictor of mortality? *Environ. Res.* **110**, 604–611 (2010).
20. Foster, J. *et al.* Quantifying the impact of heat on human physical work capacity; part II: the observed interaction of air velocity with temperature, humidity, sweat rate, and clothing is not captured by most heat stress indices. *Int. J. Biometeorol.* **66**, 507–520 (2022).
21. Zhang, Y. & Liu, C. Digital simulation for buildings' outdoor thermal comfort in urban neighborhoods. *Buildings* **11**, (2021).
22. Di Napoli, C., Barnard, C., Prudhomme, C., Cloke, H. L. & Pappenberger, F. ERA5-HEAT: A global gridded historical dataset of human thermal comfort indices from climate reanalysis. *Geosci. Data J.* **8**, 2–10 (2020).
23. Simpson, C. H., Brousse, O., Ebi, K. L. & Heaviside, C. Commonly used indices disagree about the effect of moisture on heat stress. *npj Clim. Atmos. Sci.* **6**, 1–7 (2023).
24. Hersbach, H. *et al.* ERA5 hourly data on single levels from 1940 to present. *Copernicus Climate Change Service (C3S) Climate Data Store (CDS)* (2023). https://doi.org/10.24381/cds.adbb2d47

25. Spangler, K. R., Liang, S. & Wellenius, G. A. Wet-Bulb Globe Temperature, Universal Thermal Climate Index, and Other Heat Metrics for US Counties, 2000–2020. *Sci. Data* **9**, 1–9 (2022).
26. He, C. *et al.* The effects of night-time warming on mortality burden under future climate change scenarios: a modelling study. *Lancet Planet. Heal.* **6**, e648–e657 (2022).
27. Jian, H. *et al.* A high temporal resolution global gridded dataset of human thermal stress metrics. *Sci. data* **11**, 1116 (2024).
28. Muñoz Sabater, J. ERA5-Land hourly data from 1950 to present. *Copernicus Climate Change Service (C3S) Climate Data Store (CDS)* (2019). https://doi.org/10.24381/cds.e2161bac
29. Muñoz-Sabater, J. et al. ERA5-Land: a state-of-the-art global reanalysis dataset for land applications. *Earth Syst. Sci. Data* **13**, 4349–4383 (2021).
30. Wouters, H. *et al.* Soil drought can mitigate deadly heat stress thanks to a reduction of air humidity. *Sci. Adv.* **8**, 1–11 (2022).
31. Mohammad, P. & Weng, Q. Comparing existing heat wave indices in identifying dangerous heat wave outdoor conditions. *Nexus* **1**, 100027 (2024).
32. Im, E. S., Pal, J. S. & Eltahir, E. A. B. Deadly heat waves projected in the densely populated agricultural regions of South Asia. *Sci. Adv.* **3**, 1–7 (2017).
33. Miralles, D. G., Teuling, A. J., Van Heerwaarden, C. C. & De Arellano, J. V. G. Mega-heatwave temperatures due to combined soil desiccation and atmospheric heat accumulation. *Nat. Geosci.* **7**, 345–349 (2014).
34. Hall, A. & Horta, A. Broad Scale Spatial Modelling of Wet Bulb Globe Temperature to Investigate Impact of Shade and Airflow on Heat Injury Risk and Labour Capacity in Warm to Hot Climates. *Int. J. Environ. Res. Public Health* **20**, (2023).
35. Stull, R. Wet-bulb temperature from relative humidity and air temperature. *J. Appl. Meteorol. Climatol.* **50**, 2267–2269 (2011).
36. Liljegren, J. C., Carhart, R. A., Lawday, P., Tschopp, S. & Sharp, R. Modeling the wet bulb globe temperature using standard meteorological measurements. *J. Occup. Environ. Hyg.* **5**, 645–655 (2008).
37. Bathiany, S., Dakos, V., Scheffer, M. & Lenton, T. M. Climate models predict increasing temperature variability in poor countries. *Sci. Adv.* **4**, 1–10 (2018).
38. Matthews, T. K. R., Raymond, C., Foster, J., Baldwin, J. W., Ivanovich, C., Kong, Q., Kinney, P. L., & Horton, R. M. Mortality impacts of the most extreme heat events. Nat. Rev. *Earth Environ*. **6**, 193–210 (2025). https://doi.org/10.1038/s43017-024-00635-w
39. Malik, A. et al. Accelerated historical and future warming in the Middle East and North Africa. *J. Geophys. Res. Atmos.* **129**, e2024JD041625 (2024).
40. Copernicus Climate Change Service. ERA5 hourly data on single levels from 1940 to present. *Copernicus Climate Change Service (C3S) Climate Data Store (CDS)* https://doi.org/10.24381/cds.adbb2d47 (2023).
41. Copernicus Climate Change Service. ERA5-Land hourly data from 1950 to present. *Copernicus Climate Change Service (C3S) Climate Data Store (CDS).* https://doi.org/10.24381/cds.e2161bac (2019).
42. Di Napoli, C., Barnard, C., Prudhomme, C., Cloke H. L. & Pappenberger, F. Thermal comfort indices derived from ERA5 reanalysis. *Copernicus Climate Change Service (C3S) Climate Data Store (CDS)*. https://doi.org/10.24381/cds.553b7518 (2020)

43. Yan, Y., Xu, Y. & Yue, S. A High-spatial-resolution Dataset of Human Thermal Stress Indices over South and East Asia. *figshare* https://doi.org/10.6084/m9 (2021).
44. Jian, H. *et al*. HiGTS: A high temporal resolution global gridded dataset of human thermal stress metrics. *Figshare* https://doi.org/10.6084/m9 (2024).
45. Brimicombe, C. *et al.* Thermofeel: A python thermal comfort indices library. *SoftwareX* **18**, 101005 (2022).
46. Kong, Q. & Huber, M. Explicit Calculations of Wet-Bulb Globe Temperature Compared With Approximations and Why It Matters for Labor Productivity. *Earth's Futur.* **10**, (2022).
47. Di Napoli, C., Hogan, R. J. & Pappenberger, F. Mean radiant temperature from global-scale numerical weather prediction models. *Int. J. Biometeorol.* **64**, 1233–1245 (2020).
48. Brimicombe, C. *et al.* Wet Bulb Globe Temperature: Indicating Extreme Heat Risk on a Global Grid. *GeoHealth* **7**, 1–14 (2023).
49. Kántor, N. & Unger, J. The most problematic variable in the course of human-biometeorological comfort assessment - The mean radiant temperature. *Cent. Eur. J. Geosci.* **3**, 90–100 (2011).
50. Li, X., Chakraborty, T. C. & Wang, G. Comparing land surface temperature and mean radiant temperature for urban heat mapping in Philadelphia. *Urban Clim.* **51**, 101615 (2023).
51. Staiger, H. & Matzarakis, A. Estimating down- and up-welling thermal radiation for use in mean radiant temperature. *7th Conf. Biometeorol.* **0**, 213–218 (2010).
52. Jendritzky, G., Menz, H., Schirmer, H. & Schmidt-Kessen, W. Methodik zur raumbezogenen Bewertung der thermischen Komponente im Bioklima des Menschen (Fortgeschriebenes KlimaMichel-Modell). *Beitr. Akad. Raumforsch. Landesplan.* **114** (1990).
53. Verein Deutscher Ingenieure (VDI). VDI 3787 Part 1: Environmental meteorology—methods for the human biometeorological evaluation of climate and air quality for urban and regional planning. Part I: Climate. *Beuth Verlag*, Berlin (1998).
54. Holmer, B., Lindberg, F. & Thorsson, S. Mean radiant temperature and the shape of the standing man. *10th Int. Conf. Urban Clim.* 4 (2018).
55. Halawa, E., Van Hoof, J. & Soebarto, V. The impacts of the thermal radiation field on thermal comfort, energy consumption and control - A critical overview. *Renew. Sustain. Energy Rev.* **37**, 907–918 (2014).
56. Hajizadeh, R., Farhang Dehghan, S., Golbabaei, F., Jafari, S. M. & Karajizadeh, M. Offering a model for estimating black globe temperature according to meteorological measurements. *Meteorol. Appl.* **24**, 303–307 (2017).
57. Turco, S.H.N. *et al.* Estimating black globe temperature based on meteorological data. *Livestock Environment VIII Conference*, August 31–September 4 2008, Iguassu Falls, Brazil (2009).
58. Jendritzky, G., de Dear, R. & Havenith, G. UTCI-Why another thermal index? *Int. J. Biometeorol.* **56**, 421–428 (2012).
59. Bröde, P. *et al.* Deriving the operational procedure for the Universal Thermal Climate Index (UTCI). *Int. J. Biometeorol.* **56**, 481–494 (2012).
60. Hunter, C.H. Estimating Wet Bulb Globe Temperature Using Standard Meteorological Measurements. *Proc. Conf. Environmental Applications*, 13–17 Jan 2000, Long Beach, CA, USA. WSRC-MS–99–00757, Savannah River Site.

61. Minard, D. Prevention of heat casualties in Marine Corps recruits. Period of 1955-60, with comparative incidence rates and climatic heat stresses in other training categories. *Military Medicine*, **126**, 261–272. https://doi.org/10.1093/ (1961).
62. Lin, Y. C., Jung, C. R., Hwang, B. F. & Chen, C. P. Investigating wet-bulb globe temperature on heat-related illness in general population for alerting heat exposure: A time-stratified case-crossover study. *Urban Clim.* **59**, 102322 (2025).
63. Havenith, G. & Fiala, D. Thermal indices and thermophysiological modeling for heat stress. *Compr. Physiol.* **6**, 255–302 (2016).
64. Masterson, J. & Richardson, F. A. Humidex, A Method of Quantifying Human Discomfort Due to Excessive Heat and Humidity. *Downsview, Ontario Environ. Canada* 45 (1979).
65. Li, P. W. & Chan, S. T. Application of a weather stress index for alerting the public to stressful weather in Hong Kong. *Meteorol. Appl.* **7**, 369–375 (2000).
66. Steadman R.G. A universal scale of apparent temperature. *J Clim Appl Meteorol*, 23 (12), 1674–1687 (1984)
67. Siple, M. P. A. & Army, U. S. Measurements of Dry Atmospheric Cooling in Subfreezing Temperatures Author (s): Paul A. Siple and Charles F . Passel Source : Proceedings of the American Philosophical Society , Vol . 89 , No . 1 , Reports on Scientific Results of the United States Ant. **89**, 177–199 (1945).
68. Coccolo, S., Kämpf, J., Scartezzini, J. L. & Pearlmutter, D. Outdoor human comfort and thermal stress: A comprehensive review on models and standards. *Urban Clim.* **18**, 33–57 (2016).
69. Rothfusz, L.P. The Heat Index "Equation" (or, More Than You Ever Wanted to Know About Heat Index). *NWS Southern Region Technical Attachment SR 90-23*, National Weather Service, Fort Worth, TX (1990).
70. Blazejczyk, K., Epstein, Y., Jendritzky, G., Staiger, H. & Tinz, B. Comparison of UTCI to selected thermal indices. *Int. J. Biometeorol.* **56**, 515–535 (2012).
71. Malik, A. et al. Comprehensive Heat Indices (CHI) Dataset (v1.0). *figshare* https://doi.org/10.6084/m9.figshare.30539867.v3 (2025).
72. Raei, E., Nikoo, M., AghaKouchak, A. *et al.* GHWR, a multi-method global heatwave and warm-spell record and toolbox. *Sci Data* **5**, 180206 (2018). https://doi.org/10.1038/sdata.2018.206.
73. Błazejczyk, K. *et al.* An introduction to the Universal thermal climate index (UTCI). *Geographia Polonica.* **86**, 5–10 (2013).
74. van Hove, L. W. A., Jacobs, C. M. J., Heusinkveld, B. G., Elbers, J. A., van Driel, B. L. & Holtslag, A. A. M. Temporal and spatial variability of urban heat island and thermal comfort within the Rotterdam agglomeration. *Build. Environ.* **83**, 91–103 (2015).
75. Wiszniowski, J. Healthy city versus the urban heat island effect in the context of global warming. Passive and active methods reduction of UHI. *Builder* **284**, 29–31 (2021).
76. Amini, H., Jabari, S. & McGrath, H. Assessing Future Changes in Mean Radiant Temperature: Considering Climate Change and Urban Development Impacts in Fredericton, New Brunswick, Canada, by 2050. *GeoHazards* **6**, 1–13 (2025).

77. Guo H., Teitelbaum E., Houchois N., Bozlar M., Meggers F. Revisiting the use of globe thermometers to estimate radiant temperature in studies of heating and ventilation. *Energy Build*, **180**, 83–94 (2018)
78. de Dear R. Ping-pong globe thermometers for mean radiant temperatures *Heat Vent Eng J Air Cond*, 60, 10–1 (1987)
79. National Oceanic and Atmospheric Administration (NOAA). The Heat Index Equation https://www.wpc.ncep.noaa.gov/html/heatindex_equation.shtml (2025).

Acknowledgements

The present study was funded by the Climate Change Center, King Abdullah University of Science and Technology (KAUST). Muhammad Usman was supported by Zayed University (Research Incentive Fund: RIF 23021), Abu Dhabi, UAE. The authors thank the KAUST Supercomputing Laboratory for providing computing resources. This research used the Shaheen III Supercomputer managed by the Supercomputing Core Laboratory at King Abdullah University of Science & Technology (KAUST). We thank the Climate Data Store (C3S) of the Copernicus Climate Change Service for providing the reanalysis products. This work uses, and may include modifications of, Copernicus Climate Change Service information. Neither the European Commission nor ECMWF is responsible for any use of the Copernicus information or data contained herein.

Author Contributions

A.M. – conceptualisation, data acquisition, methodology, , formal analysis, technical validation, writing – original draft; S.M. – code optimisation and development, data management, integration, pre-processing, validation, and storage, writing – review & editing; M.A.S. – code compilation, technical assistance, resources provision, writing – review & editing; Q.K. – code scripting, software, writing – review & editing; M.U. – scientific input, writing – review & editing; H.P.D. – writing – review & editing I.H. – writing – review & editing, supervision, project administration, funding acquisition.

Competing Interests

The authors declare no competing interests.

Additional Information

Correspondence and requests for materials should be addressed to A.M. (abdul.malik@kaust.edu.sa) and S.M. (sateesh.masabathini@kaust.edu.sa)

Tables

Variable	Abbreviation	Units	Source Data
Eastward component of 10 m wind	u10	m s^{-1}	ERA5-Land[28,29] https://cds.climate.copernicus.eu/datasets/reanalysis-era5-land?tab=overview
Northward component of 10 m wind	v10	m s^{-1}	〃
2 m temperature	T2m	K	〃
2 m dewpoint temperature	Td2m	K	〃
Surface pressure	sp	Pa	〃
Surface net solar radiation	Snsr	J m^{-2}	〃
Surface net thermal radiation	Sntr	J m^{-2}	〃
Surface solar radiation downwards	Ssrd	J m^{-2}	〃
Surface thermal radiation downwards	Strd	J m^{-2}	〃
Total sky direct solar radiation at the surface	Tsdsrs	J m^{-2}	ERA5[24,40] https://cds.climate.copernicus.eu/datasets/reanalysis-era5-single-levels?tab=overview

Table 1. Input variables from ERA5 and ERA5-Land used for calculating heat stress indices in the CHI dataset. Variables include wind components, surface radiation fluxes, and near-surface meteorological parameters, with their units and data sources.

Calculated Variable	**Abbreviation**	**Units**	**Source Code**	**Method**
Relative humidity	rh	%	thermofeel[45]	$rh = (\frac{e}{es}) \times 100$ $e = vapor\ pressure = 6.11 \times 10^{(\frac{7.5\times(Td2m-273.15)}{237.3+(Td2m-273.15)})}$ $es = saturated\ vapor\ pressure = 6.11 \times 10^{(\frac{7.5\times(T2m-273.15)}{237.3+(T2m-273.15)})}$
Average cosine of the solar zenith angle during only the sunlit part of the interval	$\cos\theta$	unitless	Kong et al.[46]	$\cos\theta = sin\delta sin\Phi + \frac{1}{h_{max}-h_{min}}\cos\delta\cos\Phi(\sin h_{max} - \sin h_{min})$ δ = solar declination angle Φ = geographic latitude h = hour angle Di Napoli et al.[47]
Wind speed at 10 m	ws10	m s^{-1}	Kong et al.[46]	$\mathrm{ws10} = \sqrt{(u10)^2 + (v10)^2}$ Spangler et al.[25]
Wind speed at 2 m	ws2	m s^{-1}	Kong et al.[46]	$ws2 = max\left(ws10\left(\frac{zws2}{zws10}\right)^{urb\_exp[stab\_class-1]}, 0.13\right)$ $\frac{zws2}{zws10}$: ratio of the sensor heights urb_exp: urban exponent $stab\_class$: is the atmospheric stability class and is a function of $\cos\theta$, ws10, and ssrd 0.13 is the minimum ws2 threshold See Liljegren et al.[36]
Direct radiation	dsrp	W m^{-2}	Kong et al.[46]	$dsrp = \frac{tsdsrs}{\cos\theta}\ for\ \cos\theta > 0$ Di Napoli et al.[47]

from the sun				
Ratio of direct solar radiation	fdir	unitless	Kong et al.[46]	$fdir = \frac{(ssrd - ssrdDif)}{ssrd} = \frac{tsdsrs}{ssrd};$ $fdir = \begin{cases} 0\ if\ \ \cos\theta \leq 0\ or\ fdir < 0 \\ \quad 0.9\ if\ fdir > 0.9 \end{cases}$ $tsdsrs = (ssrd - ssrdDif)$ $ssrdDif$: Diffuse component of ssrd Di Napoli et al.[47] and Yan et al.[1]
Surface thermal radiation upwards	stru	W m^{-2}		$stru = strd - sntr$ Di Napoli et al.[47]
Surface solar radiation upwards	ssru	W m^{-2}		$ssru = ssrd - snsr$ Di Napoli et al.[47]
Diffuse solar radiation	ssrdDif	W m^{-2}		$ssrdDif = ssrd - tsdsrs$ Di Napoli et al.[47]

Table 2. Derived variables and radiation parameters computed for intermediate processing in the CHI workflow. These variables are not directly available from ERA5 or ERA5-Land but were calculated using source code and methods cited.

Sr. No	**Heat Stress Metric**	**Abbreviation**	**Units**	**Input Variables**	**Method**	**Source Code**
1	Mean Radiant Temperature	Tmrt	K	ssrd, snsr, dsrp, strd, tsdsrs, sntr, $\cos\theta$	Di Napoli et. al.[47]	thermofeel[45]
2	Globe Temperature	Tg	K	T2m, Tmrt, ws2	Guo et al.[77]; de Dear[78], Brimicombe et al.[48]	thermofeel[45]
3	Universal Thermal Climate Index	UTCI	K	T2m, ws10, Tmrt, svp	Bröde et al.[59]; Di Napoli et al.[47]	thermofeel[45]
4	Natural Wet-bulb Temperature	Tnwb	K	T2m, rh, sp, ws2, ssrd, snsr, strd, sntr, fdir, $\cos\theta$	Liljegren et al.[36] method, as modified by Kong et al.[46]	Kong et al.[46]
5	Indoor Wet-Bulb Temperature	Twb	K	T2m, rh	Stull et al.[35]	thermofeel[46]
6	Indoor Lethal Heat Stress Index	Lsi	K	Twb, rh	Wouters et al.[30]	
7	Natural Lethal Heat Stress Index	Lsin	K	Tnwb, rh	Wouters et al.[30]	

8	Wet-Bulb Globe Temperature	Twbg	K	T2m, Tmrt, ws2, Td2m	Liljegren et al.[36]; Minard[61]	thermofeel[45]
9	Humidex	Hu	K	T2m, Td2m	Masterson et al.[64]	thermofeel[45]
10	Normal / Net Effective Temperature	NET	K	T2m, ws2, rh	Li et al.[65]	thermofeel[45]
11	Apparent Temperature	AP	K	T2m, rh, ws2	Steadman[66]	thermofeel[45]
12	Wind Chill	WC	K	T2m, ws2	Coccolo et al.[68]	thermofeel[45]
13	Heat Index Adjusted	HI	K	T2m, Td2m	Rothfusz[69], NOAA[79]	thermofeel[45]

Table 3. List of heat stress indices calculated in the CHI dataset, including their abbreviations, units, required input variables, computation methods, and source code used.

Figure legends/captions

Fig. 1. Spatial distribution of daily maximum values for January, averaged over 1950–2024, for all calculated heat stress indices except WC. Numbers in each subplot show global variability (minimum and maximum), highlighting regional contrasts.

Fig. 2. Same as Figure 1 but for July, showing the spatial distribution of peak summer heat stress indices over global land areas.

Fig. 3. Daily minimum and maximum values of WC for January (left column) and July (right column), averaged over 1950–2024.

Fig. 4. Comparison of daily maximum UTCI and Tmrt on June 20, 2015, across three datasets: CHI, ERA5-Heat, and HiGTS. Panels (a), (c), and (e) show UTCI values from CHI, ERA5-Heat, and HiGTS, respectively, while panels (b) and (d) present Tmrt values from CHI and ERA5-Heat, respectively. The ranges in the panel titles indicate the minimum and maximum values (in °C) across the global domain for each dataset on the specified date.

Fig. 5. Spatial distribution (left panels) and histograms (right panels) of bias between CHI and other datasets for UTCI and Tmrt on June 20, 2015. Panels (a) and (b) show UTCI and Tmrt biases

between CHI and ERA5-Heat, respectively, while panel (c) shows UTCI bias between CHI and HiGTS. Panels (d–f) show the corresponding percentage distributions of biases. The values in parentheses in the titles of panels (a–c) represent the mean bias and root mean square (RMS) error in °C. The histograms indicate the 95th and 99th percentile bias thresholds with green and magenta lines, respectively. Positive values indicate that CHI yields higher index values than HiTSEA and vice versa.

Fig. 6. Comparison of the spatial pattern of daily maximum values of various heat stress indices from CHI and HiTSEA datasets during the heatwave over South East Asia (SEA) on June 10, 2019. Panels (a–d, i–l) display indices from CHI, while panels (e–h, m–p) show the corresponding index from HiTSEA. The ranges in the panel titles indicate the minimum and maximum values (in °C) across SEA for each index on the specified date.

Fig. 7. Spatial distribution of bias between CHI and HiTSEA (CHI minus HiTSEA) datasets for daily maximum heat stress indices over SEA on June 10, 2019. The values in parentheses in each panel title denote the mean bias and RMS error in °C. Positive values indicate that CHI yields higher index values than HiTSEA and vice versa.

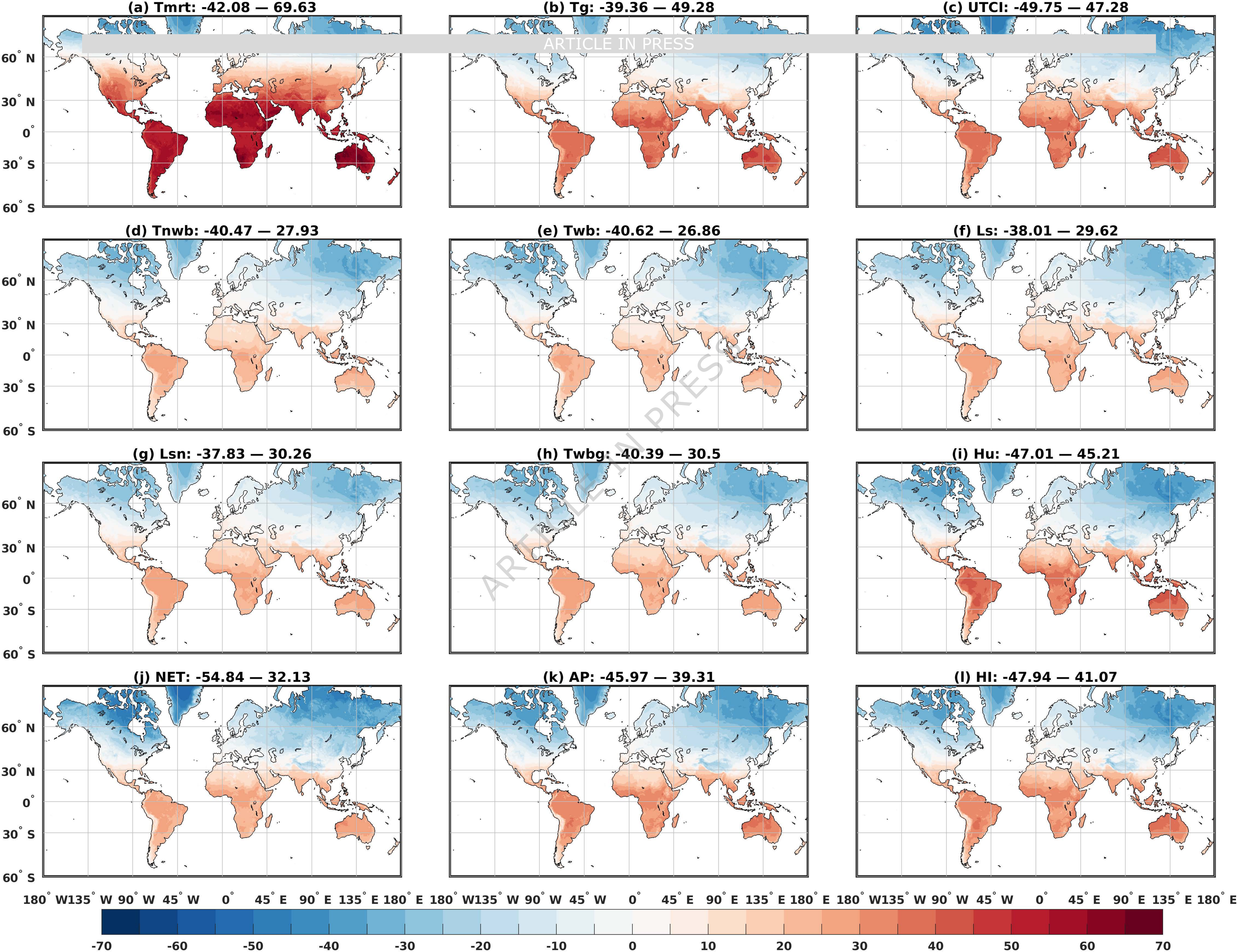

(a) Tmrt: -42.08 — 69.63
(b) Tg: -39.36 — 49.28
(c) UTCI: -49.75 — 47.28
(d) Tnwb: -40.47 — 27.93
(e) Twb: -40.62 — 26.86
(f) Ls: -38.01 — 29.62
(g) Lsn: -37.83 — 30.26
(h) Twbg: -40.39 — 30.5
(i) Hu: -47.01 — 45.21
(j) NET: -54.84 — 32.13
(k) AP: -45.97 — 39.31
(l) HI: -47.94 — 41.07
60° N
30° N
0°
30° S
60° S
180° W
135° W
90° W
45° W
0°
45° E
90° E
135° E
180° E
-70
-60
-50
-40
-30
-20
-10
0
10
20
30
40
50
60
70

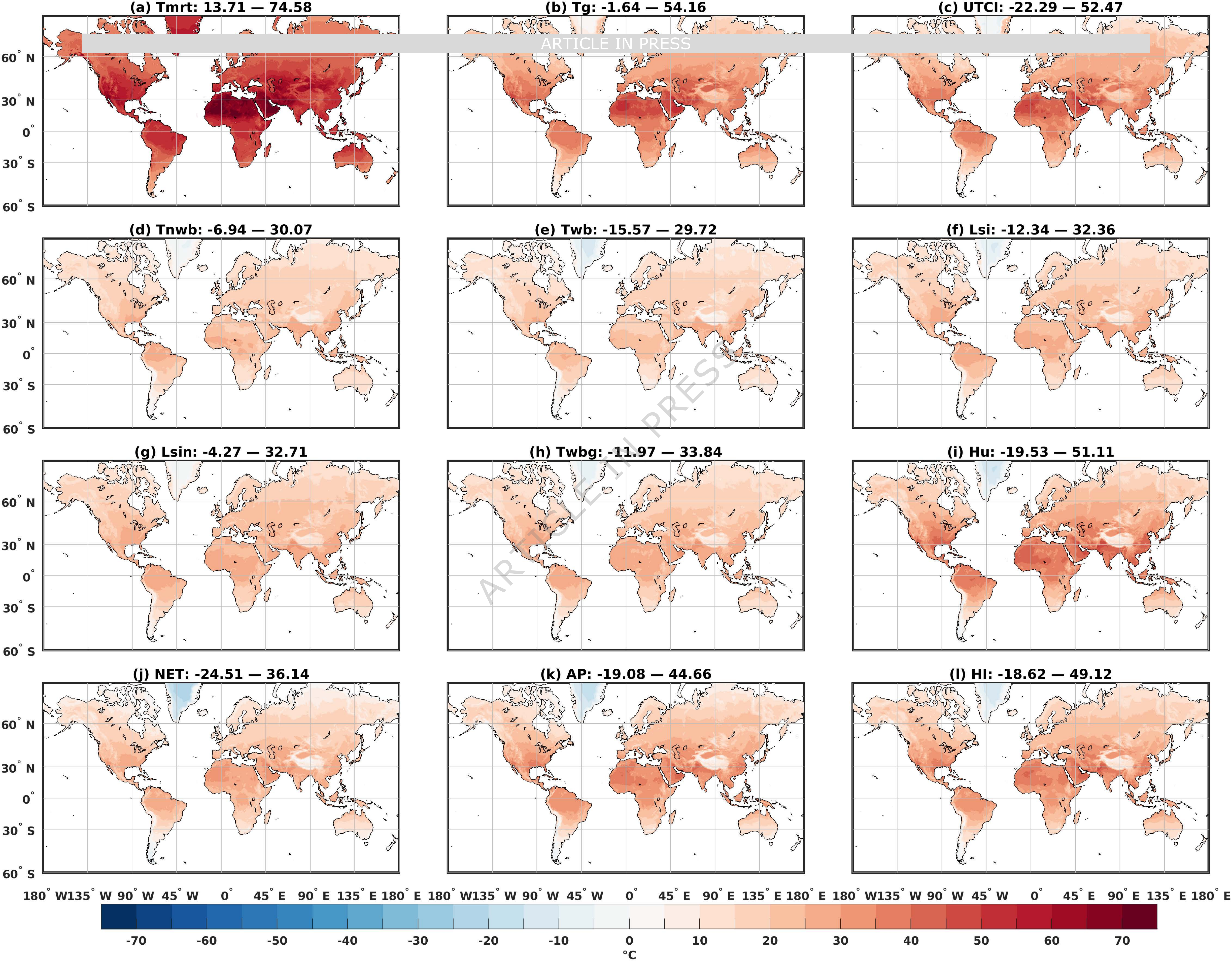
(a) Tmrt: 13.71 — 74.58
(b) Tg: -1.64 — 54.16
(c) UTCI: -22.29 — 52.47
(d) Tnwb: -6.94 — 30.07
(e) Twb: -15.57 — 29.72
(f) Lsi: -12.34 — 32.36
(g) Lsin: -4.27 — 32.71
(h) Twbg: -11.97 — 33.84
(i) Hu: -19.53 — 51.11
(j) NET: -24.51 — 36.14
(k) AP: -19.08 — 44.66
(l) HI: -18.62 — 49.12
60° N
30° N
0°
30° S
60° S
180° W 135° W 90° W 45° W 0° 45° E 90° E 135° E 180° E
-70 -60 -50 -40 -30 -20 -10 0 10 20 30 40 50 60 70
°C

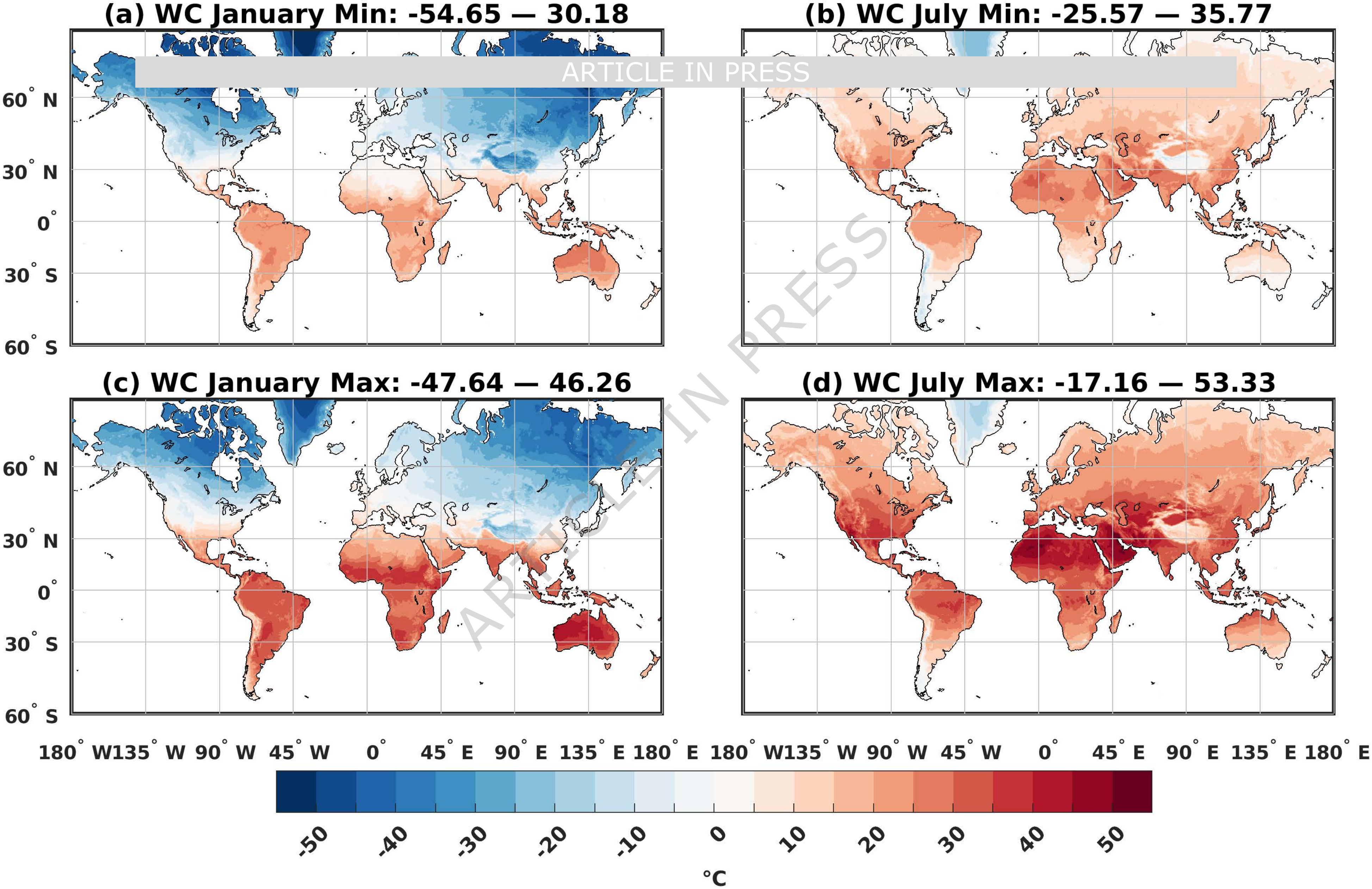

(a) WC January Min: -54.65 — 30.18
(b) WC July Min: -25.57 — 35.77
(c) WC January Max: -47.64 — 46.26
(d) WC July Max: -17.16 — 53.33
60° N
30° N
0°
30° S
60° S
180° W
135° W
90° W
45° W
0°
45° E
90° E
135° E
180° E
-50
-40
-30
-20
-10
0
10
20
30
40
50
°C

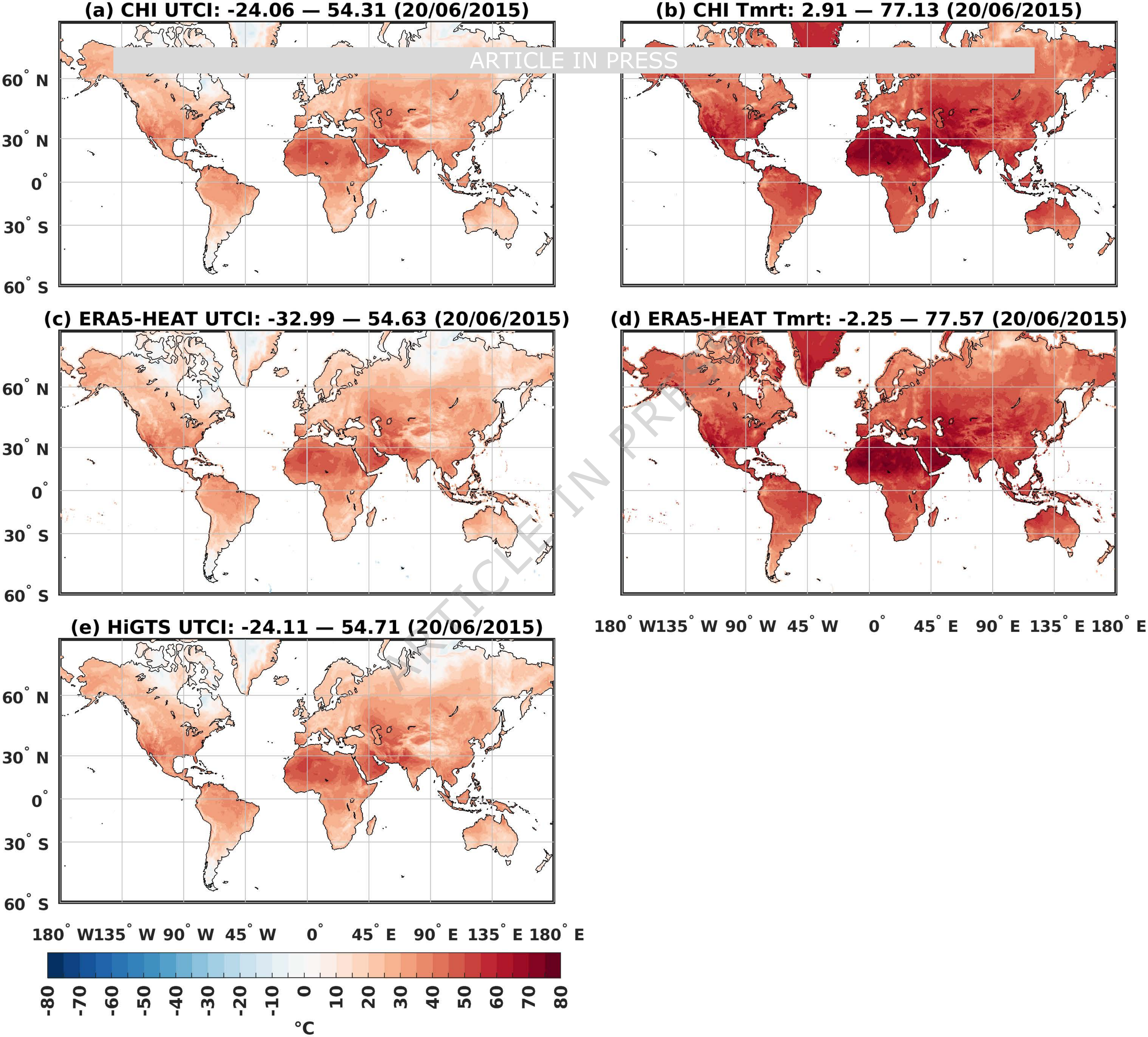
(a) CHI UTCI: -24.06 — 54.31 (20/06/2015)
(b) CHI Tmrt: 2.91 — 77.13 (20/06/2015)
(c) ERA5-HEAT UTCI: -32.99 — 54.63 (20/06/2015)
(d) ERA5-HEAT Tmrt: -2.25 — 77.57 (20/06/2015)
(e) HiGTS UTCI: -24.11 — 54.71 (20/06/2015)
60° N
30° N
0°
30° S
60° S
180° W
135° W
90° W
45° W
0°
45° E
90° E
135° E
180° E
-80
-70
-60
-50
-40
-30
-20
-10
0
10
20
30
40
50
60
70
80
°C

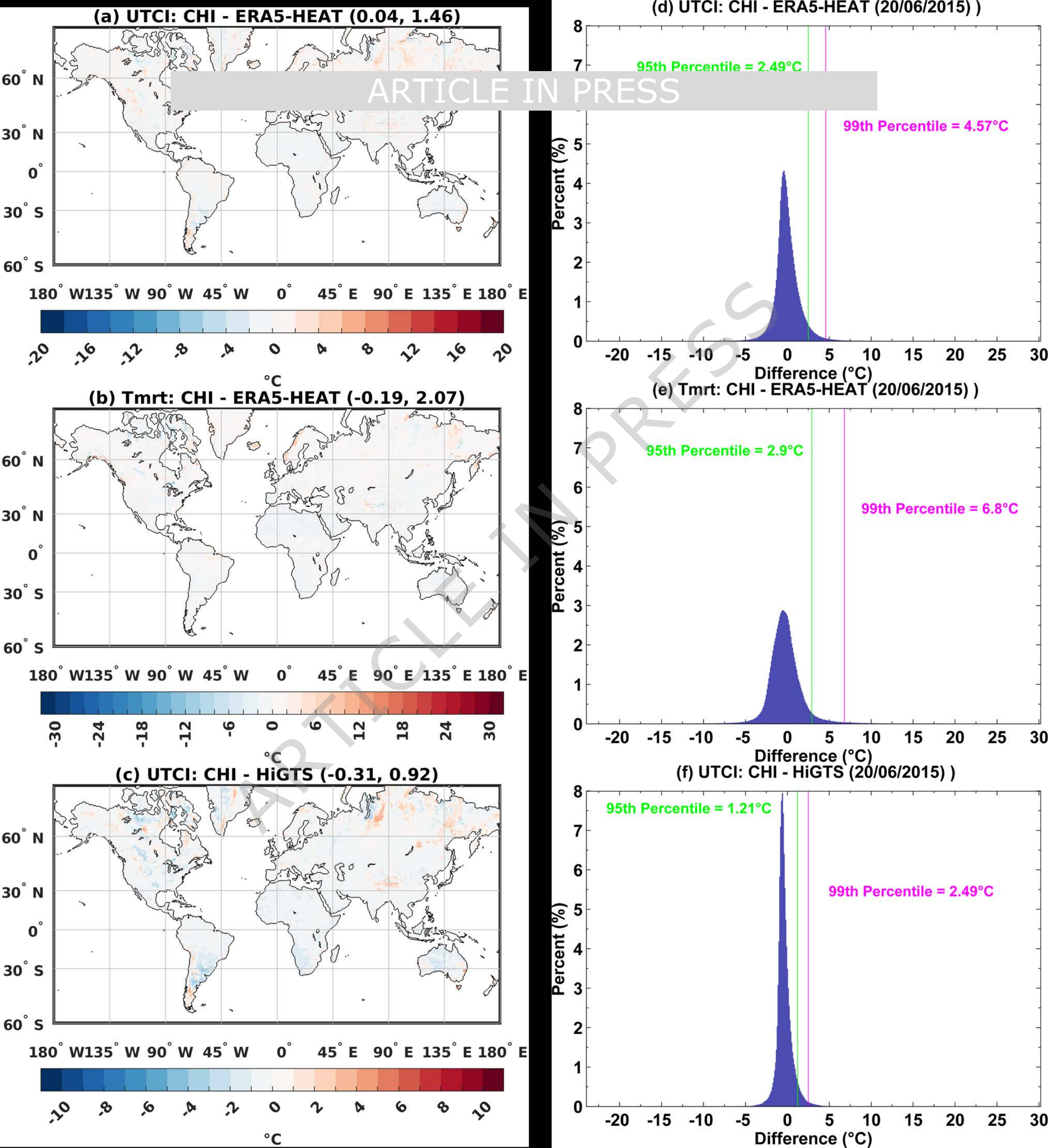
(a) UTCI: CHI - ERA5-HEAT (0.04, 1.46)
(b) Tmrt: CHI - ERA5-HEAT (-0.19, 2.07)
(c) UTCI: CHI - HiGTS (-0.31, 0.92)
60° N
30° N
0°
30° S
60° S
180° W 135° W 90° W 45° W 0° 45° E 90° E 135° E 180° E
°C
(d) UTCI: CHI - ERA5-HEAT (20/06/2015))
95th Percentile = 2.49°C
99th Percentile = 4.57°C
(e) Tmrt: CHI - ERA5-HEAT (20/06/2015))
95th Percentile = 2.9°C
99th Percentile = 6.8°C
(f) UTCI: CHI - HiGTS (20/06/2015))
95th Percentile = 1.21°C
99th Percentile = 2.49°C
Percent (%)
Difference (°C)

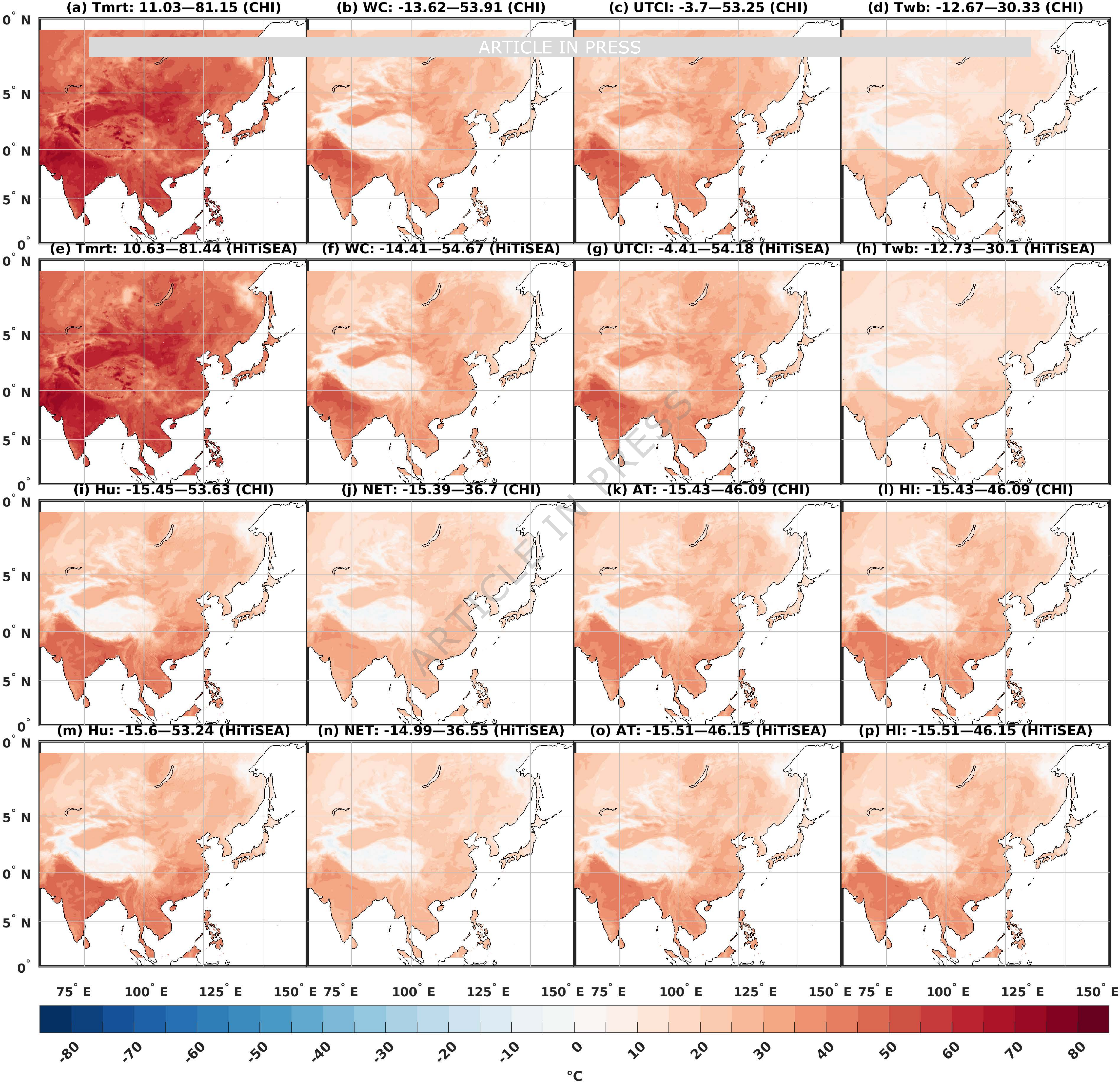
(a) Tmrt: 11.03—81.15 (CHI)
(b) WC: -13.62—53.91 (CHI)
(c) UTCI: -3.7—53.25 (CHI)
(d) Twb: -12.67—30.33 (CHI)
(e) Tmrt: 10.63—81.44 (HiTiSEA)
(f) WC: -14.41—54.67 (HiTiSEA)
(g) UTCI: -4.41—54.18 (HiTiSEA)
(h) Twb: -12.73—30.1 (HiTiSEA)
(i) Hu: -15.45—53.63 (CHI)
(j) NET: -15.39—36.7 (CHI)
(k) AT: -15.43—46.09 (CHI)
(l) HI: -15.43—46.09 (CHI)
(m) Hu: -15.6—53.24 (HiTiSEA)
(n) NET: -14.99—36.55 (HiTiSEA)
(o) AT: -15.51—46.15 (HiTiSEA)
(p) HI: -15.51—46.15 (HiTiSEA)
0° N
5° N
0° N
5° N
0°
75° E
100° E
125° E
150° E
-80
-70
-60
-50
-40
-30
-20
-10
0
10
20
30
40
50
60
70
80
°C

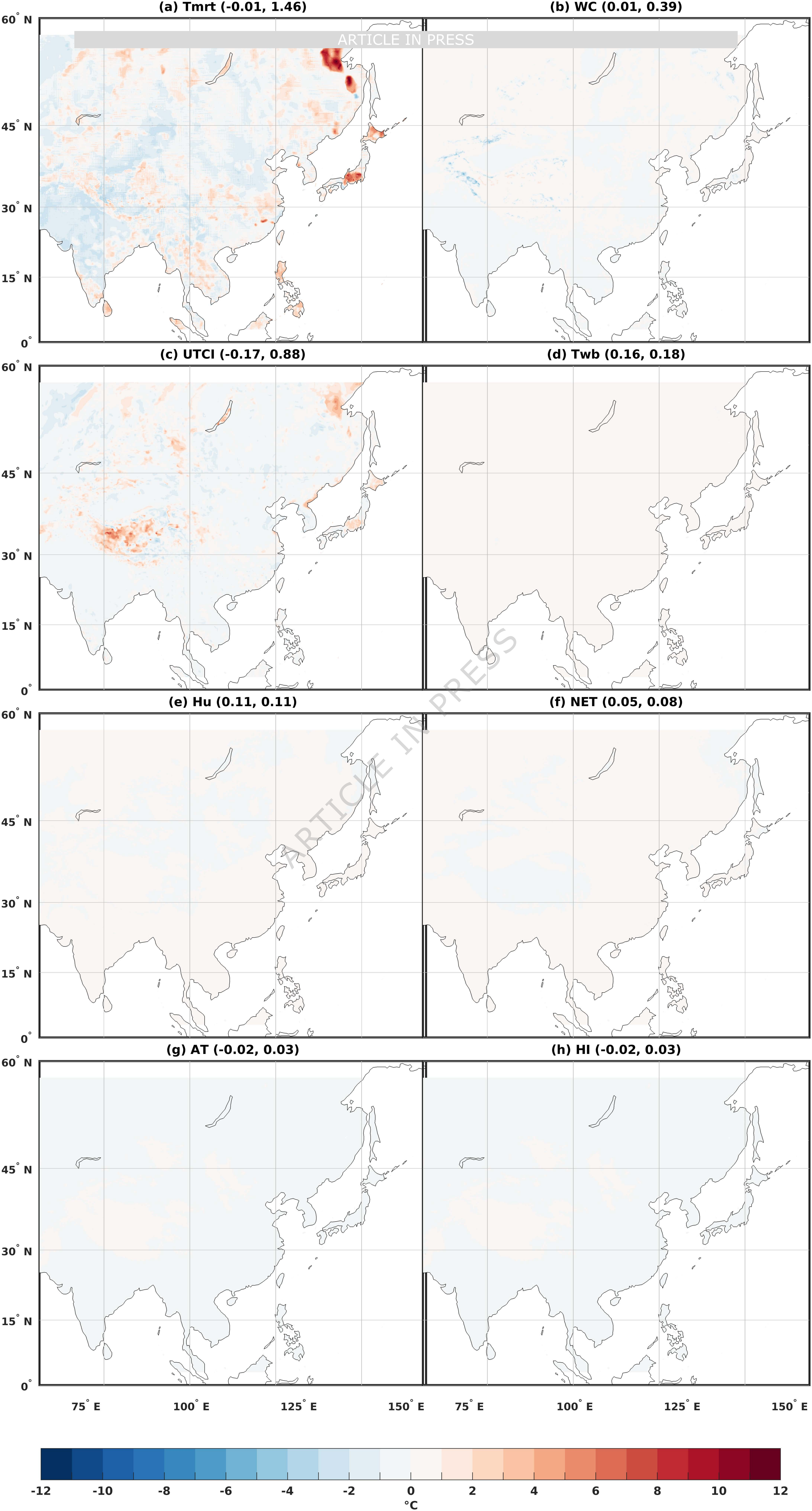

ARTICLE IN PRESS